Title
Catalytic asymmetric C–H insertion reactions of vinyl carbocations

Journal
Science, 378(6624)

ISSN
0036-8075

Authors
Nistanaki, Sepand K
Williams, Chloe G
Wigman, Benjamin
et al.

Publication Date
2022-12-09

DOI
10.1126/science.ade5320

Peer reviewed

HHS Public Access

Author manuscript

Science. Author manuscript; available in PMC 2023 March 08.

Published in final edited form as:

Science. 2022 December 09; 378(6624): 1085–1091. doi:10.1126/science.ade5320.

Catalytic asymmetric C–H insertion reactions of vinyl carbocations

Sepand K. Nistanaki[1], **Chloe G. Williams**[1], **Benjamin Wigman**[2], **Jonathan J. Wong**[2], **Brittany C. Haas**[3], **Stasik Popov**[2], **Jacob Werth**[3], **Matthew S. Sigman**[3,*], **K. N. Houk**[2,*], **Hosea M. Nelson**[1,*]

[1]Division of Chemistry and Chemical Engineering, California Institute of Technology, Pasadena, CA 91125, USA.

[2]Department of Chemistry and Biochemistry, University of California, Los Angeles, Los Angeles, CA 90095, USA.

[3]Department of Chemistry, University of Utah, Salt Lake City, UT 84112, USA.

Abstract

From the preparation of pharmaceuticals to enzymatic construction of natural products, carbocations are central to molecular synthesis. Although these reactive intermediates are engaged in stereoselective processes in nature, exerting enantiocontrol over carbocations with synthetic catalysts remains challenging. Many resonance-stabilized tricoordinated carbocations, such as iminium and oxocarbenium ions, have been applied in catalytic enantioselective reactions. However, their dicoordinated counterparts (aryl and vinyl carbocations) have not, despite their emerging utility in chemical synthesis. We report the discovery of a highly enantioselective vinyl carbocation carbon–hydrogen (C–H) insertion reaction enabled by imidodiphosphorimidate organocatalysts. Active site confinement featured in this catalyst class not only enables effective enantiocontrol but also expands the scope of vinyl cation C–H insertion chemistry, which broadens the utility of this transition metal–free C(sp^3)–H functionalization platform.

Since the late 19th century, carbocations (cationic molecules that feature an even number of electrons with a positive charge residing on one or more carbon atoms) have fascinated organic chemists because of their fundamental properties and potent modes of reactivity

*Corresponding author. hosea@caltech.edu (H.M.N.); houk@chem.ucla.edu (K.N.H.); matt.sigman@utah.edu (M.S.S.).

Author contributions: H.M.N., S.K.N., C.G.W., B.W., and S.P. designed and conducted experiments. Computational studies were conducted by J.J.W. and directed by K.N.H. Statistical modeling of data was performed by B.C.H. and J.W., and M.S.S. supervised. H.M.N., M.S.S., S.K.N., C.G.W., B.W., B.C.H., J.J.W., and J.W. prepared the manuscript.

Competing interests: The authors declare that they have no competing interests.

SUPPLEMENTARY MATERIALS

science.org/doi/10.1126/science.ade5320

Materials and Methods

Figs. S1 to S24

Tables S1 to S8

Spectral Data

References (42–102)

Data S1

(1). From agostic bonding, which is critical to our understanding of chemical structure (2, 3), to biosynthesis, in which carbocations facilitate the assembly of stereo-chemically complex natural products (4, 5), these reactive intermediates have played an essential role in our understanding of chemistry. Despite the relevance of carbocations to many modern synthetic processes, controlling the regio-, chemo-, and stereoselectivity of their reactions has proven challenging (6). This is especially true in asymmetric catalysis, in which high-energy, prochiral cationic intermediates must proceed through energetically differentiated diastereomeric transition states (TSs) to obtain synthetically useful enantiomeric excesses (ee). Achieving an energy difference ($\Delta\Delta G^{\ddagger}$) of >2.0 kcal/mol (which is required for >90% ee at 70°C) is a daunting task for such high-energy intermediates for which productive bond formation can proceed via relatively low energetic barriers (Fig. 1A). Moreover, the propensity for such intermediates to engage in unproductive side reactions further complicates the development of selective processes. This fundamental challenge is manifested in modern carbocation chemistry, in which high levels of selectivity are only routinely realized in the reactions of resonance- or heteroatom-stabilized carbocationic species (6–10). The asymmetric reactions of carbocations that are not stabilized by p-resonance remain rare (11).

Unlike resonance-stabilized tricoordinated carbocations, dicoordinated carbocations, such as aryl and vinyl cations, have thus far been excluded from the field of asymmetric catalysis (Fig. 1B). This is likely due to the lack of catalytic methods for their generation and their high reactivity once formed (12). Recent reports that these intermediates undergo facile insertion into unactivated sp^3 C–H bonds (13–20), which often creates stereogenic carbons, prompted us to investigate their application in asymmetric catalysis. In addition to the fundamental challenges associated with engaging a high-energy species in catalytic enantioselective reactions [in some cases, dicoordinated cations are computed to undergo almost barrierless insertion into alkane C–H bonds (15, 16, 20)], most catalytic C–H insertion reactions of dicoordinated carbocations have required the use of weakly coordinating anions (WCAs). These anions are notable in their weak basicity and nucleophilicity, which avoids deleterious E1 elimination or S_N1 nucleophilic substitution reactions (21). However, the few chiral WCAs that have been reported have not been successfully used in asymmetric catalysis (22, 23) because the highly ordered TSs that are required for enantioselectivity almost always rely on directional coordinative interactions. Inspired by the exquisite stereocontrol over reactive carbocations manifested within a confined enzyme active site (24) and key synthetic studies on confinement effects in selective catalysis (25, 26), we hypothesized that confinement of a dicoordinated carbocation intermediate could direct its ensuing reactivity with enantio-control. In this work, we report the discovery of a highly enantioselective C–H insertion reaction of vinyl carbocations enabled by imidodiphosphorimidate (IDPi) strong acids pioneered by List *et al.* (27, 28), which results in an organocatalytic platform for stereoselective functionalization of unactivated C(sp^3)–H bonds (Fig. 1C).

Our initial investigations focused on the intramolecular desymmetrization of a piperidinyl fragment via C–H insertion to generate bicyclic structures, given the prevalence of nitrogen-containing polycyclic scaffolds in numerous bioactive natural products (29). After exploration of various catalyst structures (Table 1), we were able to catalyze

the transformation of vinyl tosylate **1a** to the cyclized C–H insertion product **2a** with high ee using IDPi **8B** and stoichiometric allyltriisopropylsilane (entry 6). This C–H functionalization reaction forges three contiguous stereocenters with notable diastereoselectivity [>20:1 diastereomeric ratio (d.r.)] and reasonable conversion after 72 hours. We posit that the reaction is sluggish because of a high barrier for vinyl carbocation formation and therefore is directly dependent on the Lewis acidity of the silicon species (12). Thus, we hypothesized that the conversion could be improved by tuning the silyl group on the allyl silane, given that the silylated IDPi is likely the active catalyst (see below). We were inspired by Lambert's studies on the effects of steric bulk on silylium ion coordination, in which tris(trimethylsilyl)silylium [$Si(TMS)_3^+$] paired with a WCA generated a near-trivalent silylium cation, in contrast to trialkyl silylium cations that form tetravalent Si centers by coordination to solvent or counteranion (30). Gratifyingly, in our system, we observed a positive correlation between silane size and activity (entries 6 to 8 in Table 1), in which tris(triethylsilyl) allylsilane resulted in full conversion without any influence on enantioselectivity. We performed Gutmann-Beckett studies that supported the enhanced Lewis acidity of tris(triethylsilyl)silane [$Si(TES)_3$]–silylated IDPi relative to its trialkyl silyl IDPi counterpart, although other effects cannot be ruled out (see supplementary materials).

With this improved activity and encouraging enantioselectivity on our model substrate, we explored the scope of this reaction (Fig. 2). The transformation proved compatible with substitution at both of the aryl rings on the substrate, delivering insertion products in moderate to good yield with excellent enantioselectivity (up to 93% ee) and diastereoselectivity (>20:1 d.r.). High levels of enantioselectivity were maintained with ortho substitution near the insertion site (**2g** and **2i**), with electron-rich (**2f**, **2g**, and **2o**), electron-deficient (**2e**, **2n**, and **2p**), and heterocyclic (**2j** and **2k**) substrates also performing well. Moreover, functional groups labile in many transition metal–catalyzed processes (**2p** to **2s**) were compatible, which highlights this method's complementarity to transition metal–catalyzed C(sp^3)–H functionalization platforms. C–H insertion adjacent to a sterically congested all-carbon quaternary center (**2u**) occurred in good yield, albeit with moderate enantioselectivity. An additional highlight was the conversion of an all-hydrocarbon variant of the model substrate to bicyclo[4.3.0]nonenes in modest stereoselectivity (**2v)**. The enantiopurity of many of the piperidine insertion products could be readily upgraded via a single recrystallization to afford enantiopure material (>99% ee). Moreover, the *N*-triflyl protecting group could be removed with sodium bis(2-methoxyethoxy)aluminum hydride (Red-Al) to afford free amine **2w** (31). Heating insertion product 2a with acid isomerized the olefin to the thermodynamically more favored tetrasubstituted olefin isomer (**2x**), without loss of enantioenrichment. WCA catalysts that were previously used in our laboratory in vinyl cation C–H insertion reactions resulted in low yields (<10%) or intractable product mixtures because of the formation of multiple isomers, oligomeric products, and other unidentifiable side products (see supplementary materials). These findings, when compared with previous examples of catalytic vinyl cation C–H insertion reactions, highlight a compelling advance in substrate compatibility and catalyst control.

Confirming the intermediacy of the vinyl cation

Although catalytic vinyl cation formation via sulfonate abstraction has been previously reported (15, 16), we sought to further support its intermediacy in this system. To this end, we found that both the *Z*- and *E*-vinyl tosylate isomers afforded the same insertion product with identical enantioselectivities, which supports the common intermediacy of a linear vinyl carbocation (Fig. 3A). Moreover, we prepared tosylate **9** (which cannot undergo intramolecular C–H insertion) and found that allene **10** is produced as the major product under the reaction conditions, which likely arises from a Wagner-Meerwein rearrangement —a known reactivity pathway of vinyl carbocations (12).

In the context of enantioselective insertion, the allyl silane did not influence the selectivity of the reaction, despite its profound influence on rate. This result not only supports the proposed role of the Si-center in the ionization of the substrate but also suggests that after ionization, a discrete vinyl cation–IDPi ion pair is formed that undergoes the enantiodetermining C–H insertion step. Supporting this hypothesis, deuteration of the substrate's insertion sites resulted in an appreciable increase in % ee across two structurally distinct catalysts (Fig. 3B), which corresponds to up to a 0.12 ± 0.03 kcal/mol difference in $\Delta\Delta G^{\ddagger}$ (32). Moreover, no indication of deuterium incorporation adjacent to the CD_2 methylene was observed, which would be expected if a stepwise hydride rebound mechanism was operative (15) given that hydride shifts would result in H/D scrambling (Fig. 3C). Additionally, substrate **1u** cleanly forms insertion product **2u** in high yield, with no sign of rearrangement. Although these observations support either a concerted insertion or a rapid rebound mechanism, in which a putative 2° carbocation is trapped by olefin attack before facile 1,2-shifts can occur, we recognize that the mechanism likely resides on a continuum between these two extreme scenarios (see below). On the basis of these results, a proposed mechanism (Fig. 3D) initiates with protodesilylation of the allylsilane to generate the active Lewis acid **11**, which is consistent with prior work by List *et al.* (27, 33). Subsequent ionization of the vinyl tosylate by **11** generates the reactive vinyl cation species (12), which we propose is confined within the IDPi anion as a contact ion pair. An enantiodetermining C–H insertion step followed by kinetic deprotonation delivers insertion product **2** and regenerates IDPi.

Modeling the TS

To probe the specific interactions responsible for the experimentally observed stereoselectivity, density functional theory (DFT) calculations at the ωB97X-D/6–311++G(d,p), CPCM(cyclohexane)//B3LYP-D3/6–31G(d,p), CPCM(cyclohexane) level were carried out. Two diastereomeric TSs that used substrate **1a** and catalyst **8B** were computed and found to correspond with a concerted, asynchronous C–H insertion of the vinyl cation with an energy difference ($\Delta\Delta G^{\ddagger}$) of 2.1 kcal/mol, which favored the experimentally observed enantiomer (Fig. 3E). In the minor TS, the sterically encumbering piperidine is situated in much closer proximity to the congested *p*-SF_5 substituents of the catalyst scaffold. These repulsive interactions obstruct the optimal positioning of the substrate within the anionic pocket of the catalyst, which ultimately weakens the intermolecular interactions between the associated ions. The difference in electrostatic stabilization between the two TSs was calculated to be

0.6 kcal/mol (34) with an additional 1.4 kcal/mol of stabilization in the favored enantiomeric TS arising from dispersive interactions, which together correspond to enhanced binding of the C–H insertion TS by the IDPi anion if the preferred enantiomeric conformation is adopted. Careful inspection of the TS structure reveals bending of the vinyl cation, placing the tolyl group away from the bulky N–Tf piperidine ring (Tf, trifluoromethylsulfonyl), which is consistent with an anti relative orientation seen in the experimentally obtained diastereomer. Although product **2a** was computed to be energetically favored over its benzylic epimer (**14**; Fig. 3F), thermodynamically driven equilibration after C–H insertion is likely not the driver of diastereoselectivity. 1,2-hydride shifts are known to be stereospecific (35), which rules out benzylic hydride exchange as a potential mechanism for epimerization of the benzylic stereocenter (Fig. 3F), and hydride shifts from the ring fusion carbon are discounted given the lack of H/D scrambling observed in deuterated substrate **1b**–$\mathbf{D_4}$ (Fig. 3C). Taken together, these results are consistent with a 1,1-insertion step that sets all three stereocenters concurrently with high stereocontrol (see supplementary materials for further discussion).

To further explore factors governing how catalyst and substrate structure affected the enantioselective outcomes, we investigated the reaction holistically by using statistical modeling to analyze the diverse reaction outputs recorded within the optimization and substrate scope studies. This was accomplished by regressing computationally derived molecular descriptors to the measured enantioselectivities (36). Substrates and truncated IDPi catalysts (see supplementary materials) were independently subjected to conformational searches by using molecular mechanics, and the relevant structures were submitted for DFT optimization at the PBE1PBE-D3BJ/def2-SVP level of theory with M06–2X/def2-TZVP single-point energy corrections. Both steric and electronic molecular descriptors were extracted from the lowest energy conformer of the computed ensembles (37). The data were split into a training and validation set by using a pseudorandom 50:50 partition followed by forward stepwise multivariate linear regression analysis. A four-parameter model [coefficient of determination (R^2) = 0.85] was found in which (Fig. 4A) two features for both the catalyst and substrate are required for a good correlation (Fig. 4B). Cross-validation techniques, including leave one out (LOO; 0.79) and k-fold (k = 4,0.77), as well as external validation [predicted R^2 ($_{pred}R^2$) = 0.77], were performed to indicate that a statistically robust model was produced. The catalyst is described by the natural bond orbital (NBO) partial charge of the para substituent and the buried volume within a 3.5-Å sphere centered on the sulfonamide sulfur ($VBur_S$), which indicates that a more sterically constricted catalyst pocket positively affects selectivity, consistent with the DFT TS studies. The substrate is described by the ^{13}C nuclear magnetic resonance (NMR) chemical shift and partial equalization of orbital electronegativity (PEOE), which are both primarily electronic descriptors (38). The PEOE term can classify general substrate types as well as differentiate the various piperidine protecting groups that were tested during optimization [i.e., *p*-toluenesulfonyl (Ts), Tf, trifluoroacetyl (TFA), and so on] on the basis of the proximity of electronegative atoms (Fig. 4C). Taken together, this model suggests that high enantioselectivity results from a combination of sterically restricted catalysts and dense electronegativity present in the Tf-protected piperidinyl substrates. Catalysis is optimal in the negatively charged pocket of the catalyst for substrates with cation stabilization features,

which rationalizes the 93% ee we observed for IDPi (**8B**) with **2f** and supporting the proposed TS.

Extension to strained-ring product motifs

Having established the conceptual groundwork for achieving enantioselectivity in a vinyl cation C(sp^3)–H insertion reaction, we sought to test our system with new substrate classes, and we were particularly drawn to the possibility of leveraging the high energy of these intermediates to forge strained rings. Bicyclo[3.2.1]octanes are prevalent carbocyclic scaffolds found in various bioactive natural products (39), and we sought to access them in enantioenriched form. To this end, we prepared substrates of the type **15** (Fig. 5), for which insertion into the cyclohexyl group generates a chiral [3.2.1] carbocycle (16), and found that IDPi **3A** (Table 1) catalyzes its formation in moderate yields and enantioselectivity (up to 77% ee). Expansion of this chemistry to other substrate classes that generate structurally distinct products suggests the potential for broader applicability of IDPi catalysis in carrying out challenging enantioselective C(sp^3)–H functionalization reactions via vinyl carbocations. Moreover, products from this reaction can be readily converted to enantioenriched 1,3-diketocyclohexanes (17) via oxidative cleavage (40) with high levels of enantiospecificity. Current catalytic methods to access enantioenriched 1,3-diketocyclohexanes are limited to the desymmetrization of anhydrides (41), after which additional steps are required to convert the resulting carboxylic acid to scaffolds such as **17a** to **17c**, which highlights a strategic application of this reaction.

Supplementary Material

Refer to Web version on PubMed Central for supplementary material.

ACKNOWLEDGMENTS

We thank S. Virgil, B. Stoltz, and S. Reisman for instrumentation; M. Shahgholi for mass spectrometry support; D. Vander Velde for NMR expertise; and M. Takase and S. Khan for x-ray crystallography analysis. Work by the Houk group used computational and storage services associated with the Hoffman2 Shared Cluster provided by UCLA Institute for Digital Research and Education's Research Technology Group. The Sigman Group's computational work was supported by the Center for High Performance Computing at the University of Utah.

Funding:

Financial support for this work was provided by the National Institutes of Health National Institute of General Medical Sciences (R35 GM12893 to H.M.N. and R35 GM136271 to M.S.S.) and the National Science Foundation (CHE-1764328 to K.N.H.; DGE-1650604 to B.W. and S.P.). S.K.N. thanks the US Public Health Service (USPHS) National Research Service Award (T32GM008496). We thank the Beckman Institute (support of the Caltech Center for Catalysis and Chemical Synthesis and the x-ray crystallography facility), the Dow Next-Generation Educator Fund (grant to Caltech), and the UCLA Molecular Instrumentation Center for NMR instrumentation and x-ray crystallography.

Data and materials availability:

All crystallographic data are available free of charge from the Cambridge Crystallographic Data Centre under CCDC 2201595, CCDC 2201596, CCDC 2201597, CCDC 2201598, CCDC 2201599, and CCDC 2201600. All other data are provided in the supplementary materials.

REFERENCES AND NOTES

1. Olah GA, J. Org. Chem 66, 5943–5957 (2001). [PubMed: 11529717]
2. Olah GA, J. Am. Chem. Soc 94, 808–820 (1972).
3. Brown HC, The Nonclassical Ion Problem (Plenum Press, 1977).
4. Eschenmoser A, Ruzicka L, Jeger O, Arigoni D, Helv. Chim. Acta 38, 1890–1904 (1955).
5. Tantillo DJ, Nat. Prod. Rep 28, 1035–1053 (2011). [PubMed: 21541432]
6. Naredla RR, Klumpp DA, Chem. Rev 113, 6905–6948 (2013). [PubMed: 23819438]
7. Wendlandt AE, Vangal P, Jacobsen EN, Nature 556, 447–451 (2018). [PubMed: 29695848]
8. Isomura M, Petrone DA, Carreira EM, J. Am. Chem. Soc 141, 4738–4748 (2019). [PubMed: 30785741]
9. Braun M, Kotter W, Angew. Chem. Int. Ed 43, 514–517 (2004).
10. Brak K, Jacobsen EN, Angew. Chem. Int. Ed 52, 534–561 (2013).
11. Properzi R et al., Nat. Chem 12, 1174–1179 (2020). [PubMed: 32989271]
12. Stang PJ, Rappoport Z, Dicoordinated Carbocations (Wiley, 1997).
13. Shao B, Bagdasarian AL, Popov S, Nelson HM, Science 355, 1403–1407 (2017). [PubMed: 28360325]
14. Mascarelli L, Gazz. Chim. Ital 66, 843–850 (1936).
15. Popov S et al., Science 361, 381–387 (2018). [PubMed: 30049877]
16. Wigman B et al., J. Am. Chem. Soc 141, 9140–9144 (2019). [PubMed: 31082208]
17. Cleary SE, Hensinger MJ, Brewer M, Chem. Sci 8, 6810–6814 (2017). [PubMed: 29147505]
18. Biermann U, Koch R, Metzger JO, Angew. Chem. Int. Ed 45, 3076–3079 (2006).
19. Zhang F et al., J. Am. Chem. Soc 136, 8851–8854 (2014). [PubMed: 24905079]
20. Cleary SE et al., J. Am. Chem. Soc 141, 3558–3565 (2019). [PubMed: 30758200]
21. Riddlestone IM, Kraft A, Schaefer J, Krossing I, Angew. Chem. Int. Ed 57, 13982–14024 (2018).
22. De CK, Mitra R, List B, Synlett 28, 2435–2438 (2017).
23. Pommerening P, Oestreich M, Eur. J. Org. Chem 2019, 7240–7246 (2019).
24. Wendt KU, Lenhart A, Schulz GE, J. Mol. Biol 286, 175–187 (1999). [PubMed: 9931258]
25. Mitschke B, Turberg M, List B, Chem 6, 2515–2532 (2020).
26. Hong CM, Bergman RG, Raymond KN, Toste FD, Acc. Chem. Res 51, 2447–2455 (2018). [PubMed: 30272943]
27. Kaib PSJ, Schreyer L, Lee S, Properzi R, List B, Angew. Chem. Int. Ed 55, 13200–13203 (2016).
28. Schreyer L, Properzi R, List B, Angew. Chem. Int. Ed 58, 12761–12777 (2019).
29. Fattorusso E, Taglialatela-Scafati O, Modern Alkaloids: Structure, Isolation, Synthesis and Biology (Wiley, 2007).
30. Lambert JB, Zhang S, Ciro SM, Organometallics 13, 2430–2443 (1994).
31. Miyamoto K, Hoque MM, Ogasa S, J. Org. Chem 77, 8317–8320 (2012). [PubMed: 22873762]
32. Neel AJ, Milo A, Sigman MS, Toste FD, J. Am. Chem. Soc 138, 3863–3875 (2016). [PubMed: 26967114]
33. Zhou H et al., J. Am. Chem. Soc 142, 13695–13700 (2020). [PubMed: 32786813]
34. Wagen CC, Kwan EE, cctk (2020); www.github.com/ekwan/cctk.
35. Dickschat JS, Nat. Prod. Rep 33, 87–110 (2016). [PubMed: 26563452]
36. Santiago CB, Guo J-Y, Sigman MS, Chem. Sci 9, 2398–2412 (2018). [PubMed: 29719711]
37. Guo J-Y, Minko Y, Santiago CB, Sigman MS, ACS Catal. 7, 4144–4151 (2017).
38. Gasteiger J, Marsili M, Tetrahedron 36, 3219–3228 (1980).
39. Presset M, Coquerel Y, Rodriguez J, Chem. Rev 113, 525–595 (2013). [PubMed: 23082820]
40. Miao M et al., Org. Lett 21, 5957–5961 (2019). [PubMed: 31298027]
41. Cook MJ, Rovis T, J. Am. Chem. Soc 129, 9302–9303 (2007). [PubMed: 17622150]

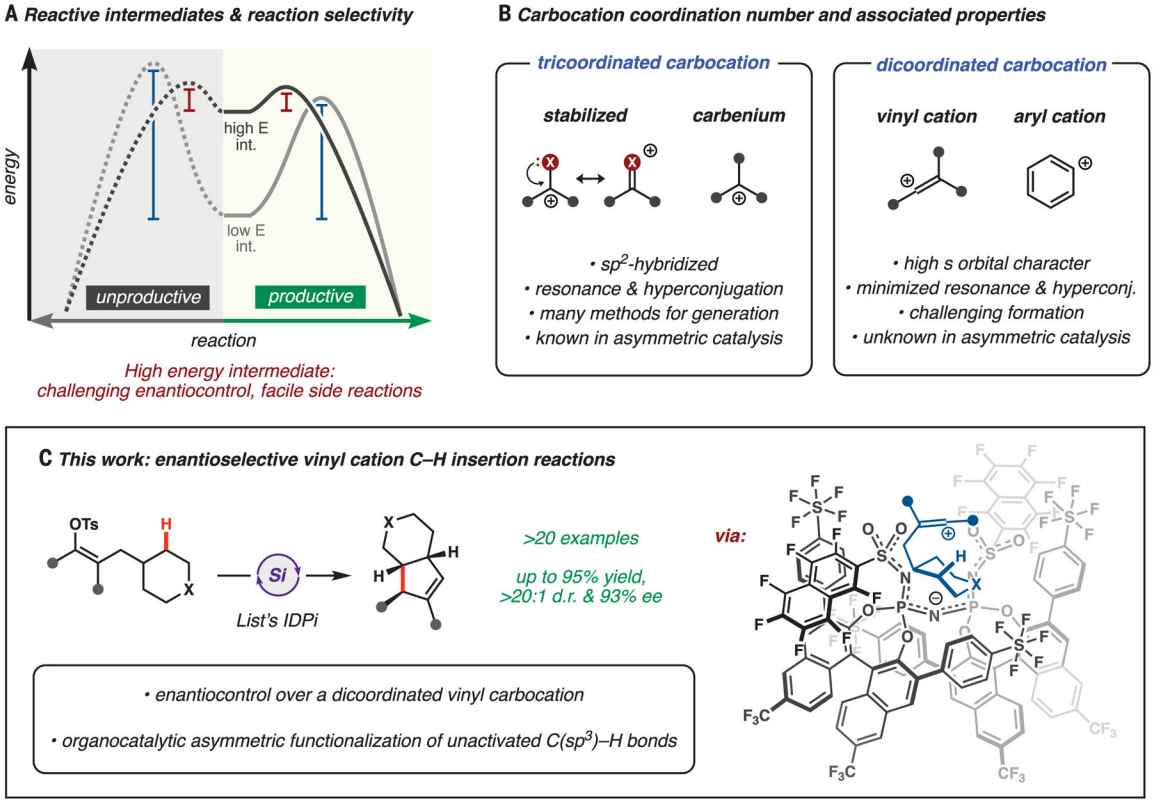

Fig. 1. Selective reactions of carbocations.

(**A**) Challenges associated with high-energy intermediates in selective catalysis. (**B**) Properties associated with carbocation coordination number. (**C**) Discovery of enantioselective C–H insertion reactions of vinyl cations. high E int, high-energy intermediate; low E int, low-energy intermediate; OTs, *p*-toluenesulfonate; X, NSO_2CF_3 or CH_2.

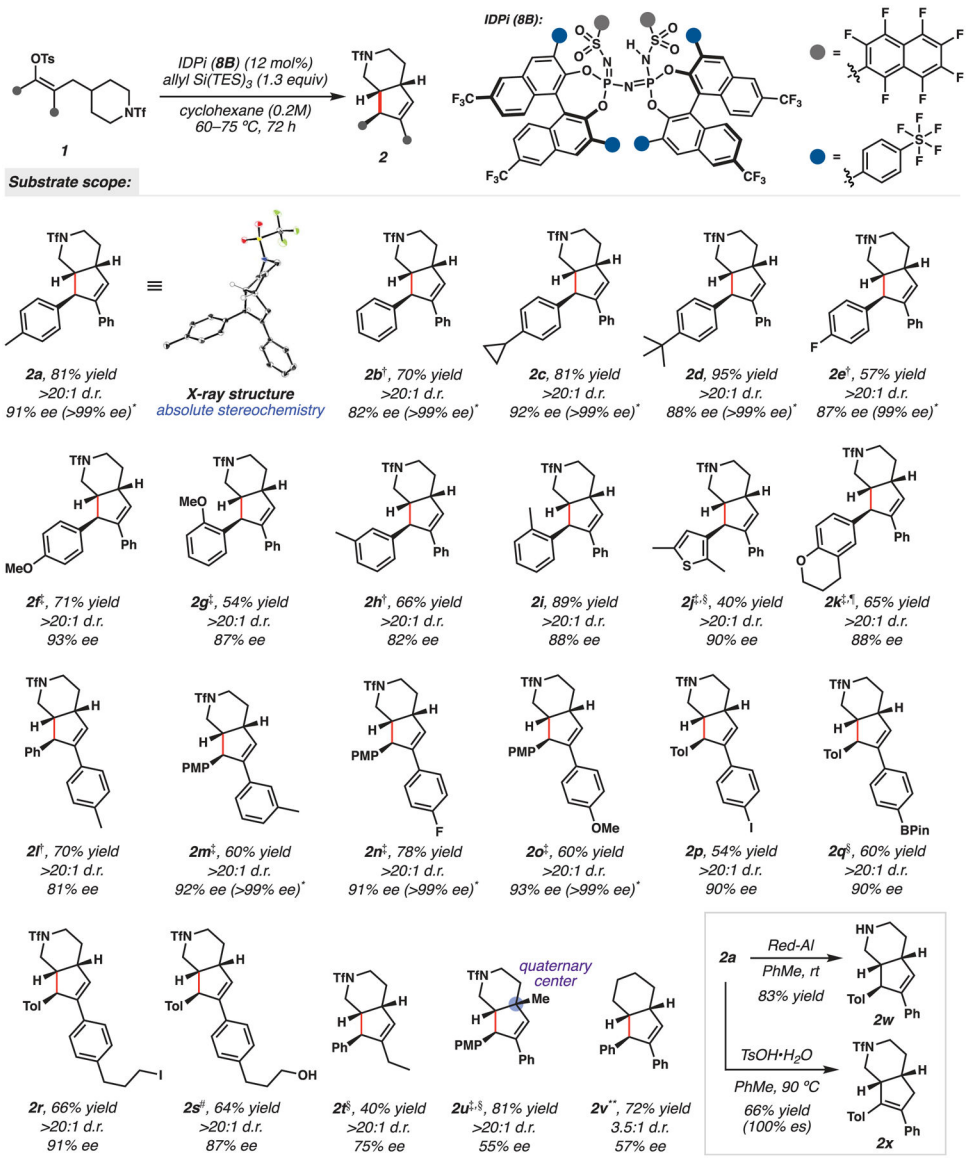

Fig. 2. Substrate scope.

All reported yields are isolated yields of purified product. *After single recrystallization. †96 hours at 75°C. ‡0.1M. §70°C. ¶60°C. #2.3 equivalents of silane used because of alcohol silylation; the crude reaction was then stirred with tetrabutylammonium fluoride. **0.025M using **3A**. BPin, pinacol boronic ester; es, enantiospecificity; Me, methyl; Ph, phenyl; PhMe, toluene; PMP, *p*-methoxyphenyl; rt, room temperature; Tol, *p*-tolyl; TsOH, *p*-toluenesulfonic acid.

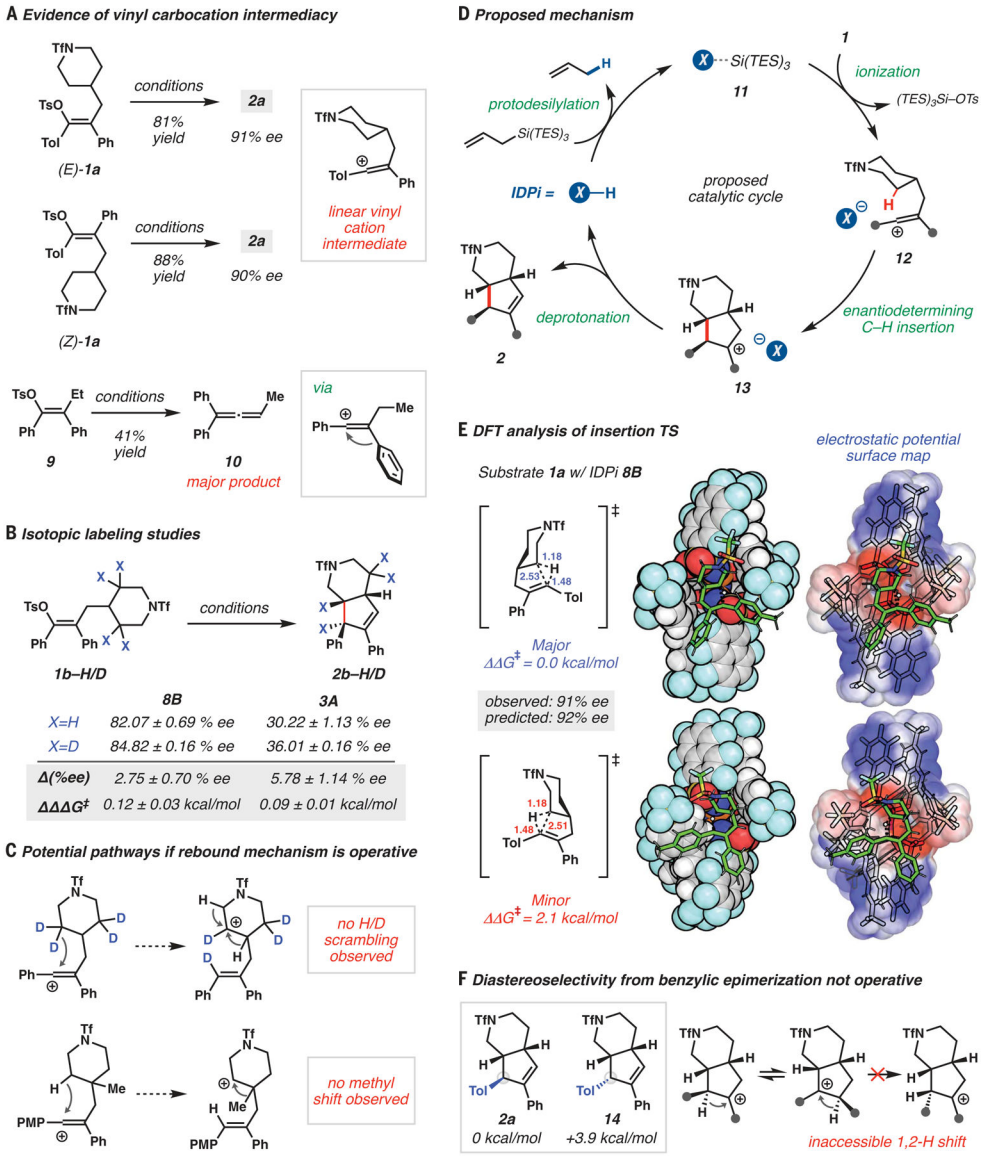

Fig. 3. Mechanistic studies.

(**A**) Evidence for vinyl carbocation intermediacy. (**B**) Effect of isotopic labeling on enantioselectivity. Listed values are the average of triplicate runs. (**C**) Rearrangement products from a rebound mechanism that were not observed. (**D**) Proposed mechanism. (**E**) DFT-calculated diastereomeric TS structures with corresponding bond lengths (Å), electrostatic potential surfaces, and free-energy differences between major and minor TSs. Substrate atoms are rendered as a stick model, and the catalyst is rendered as a space-filling model. Electrostatic potential areas are colored red to indicate a more-negative potential and blue to indicate a more-positive potential. (**F**) Benzylic stereocenter epimerization is not likely. Et, ethyl.

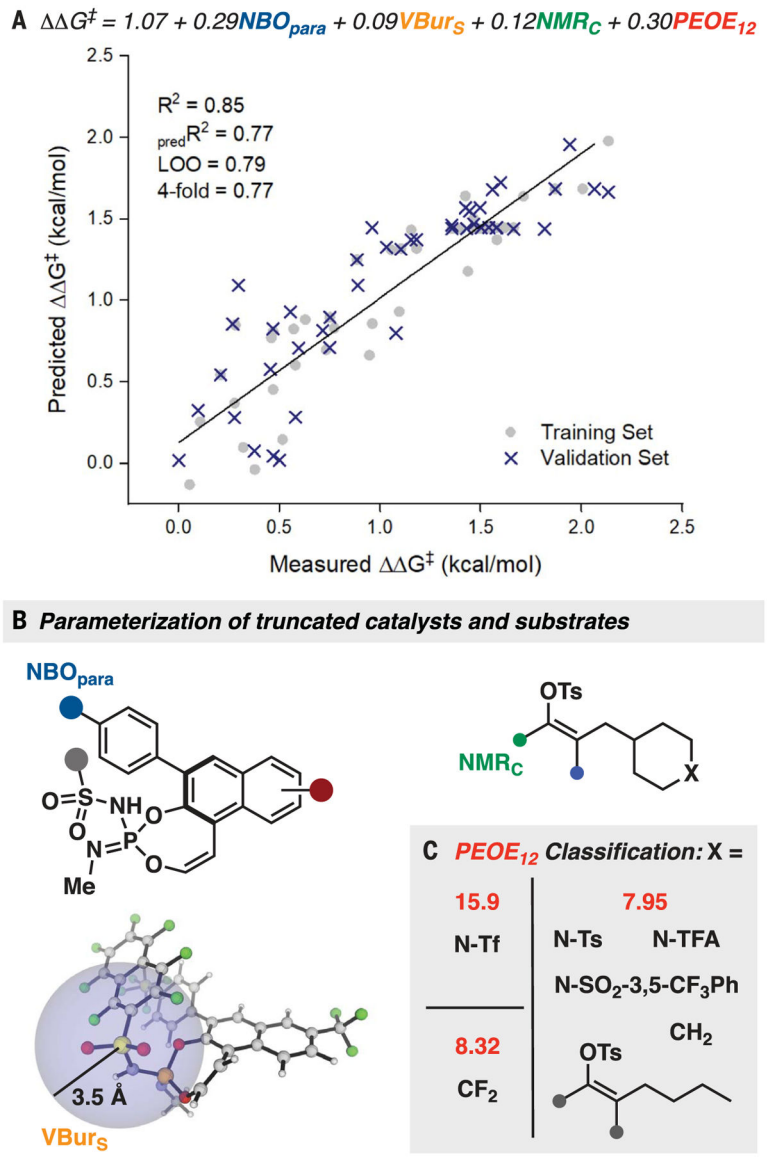

Fig. 4. Statistical modeling.

(**A**) Multivariate linear regression model with a pseudorandom 50:50 partitioning of the 91 data points into training set:validation set. (**B**) Visual representation of the molecular descriptors used in the model. (**C**) Substrate classification of X identity on the basis of $PEOE_{12}$.

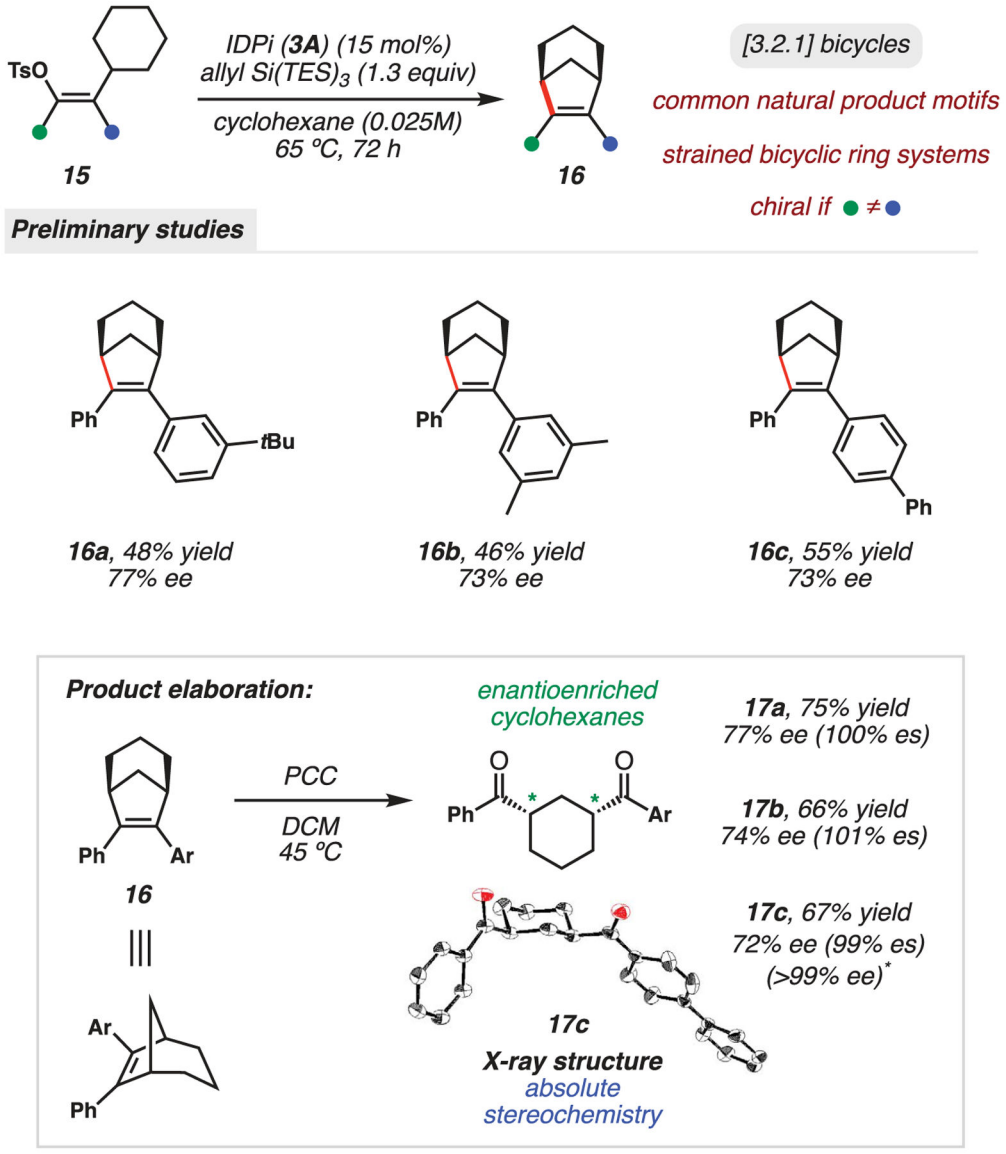

Fig. 5. Catalytic asymmetric synthesis of strained bicycles.

All reported yields are isolated yields. *After single recrystallization. Ar, aryl; DCM, dichloromethane; PCC, pyridinium chlorochromate; *t*Bu, *tert*-butyl.

Table 1.

Reaction optimization.

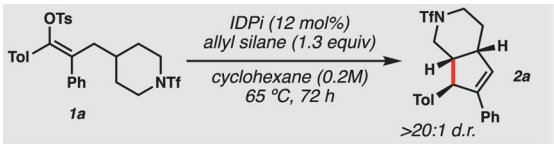

Entry	IDPi	X	Silane	Conv.	Yield	%ee
1	3A	H	allyl TIPS	70%	56%	52%
2	4B	CF_3	allyl TIPS	89%	79%	85%
3	5B	CF_3	allyl TIPS	95%	72%	60%
4	6B	CF_3	allyl TIPS	13%	11%	84%
5	7B	CF_3	allyl TIPS	93%	84%	85%
6	8B	CF_3	allyl TIPS	81%	72%	91%
7	8B	CF_3	allyl TMS	38%	34%	89%
8	8B	CF_3	allyl $Si(TES)_3$	full	91% (81%)*	91%
9	8B	CF_3	none	0%	0%	—

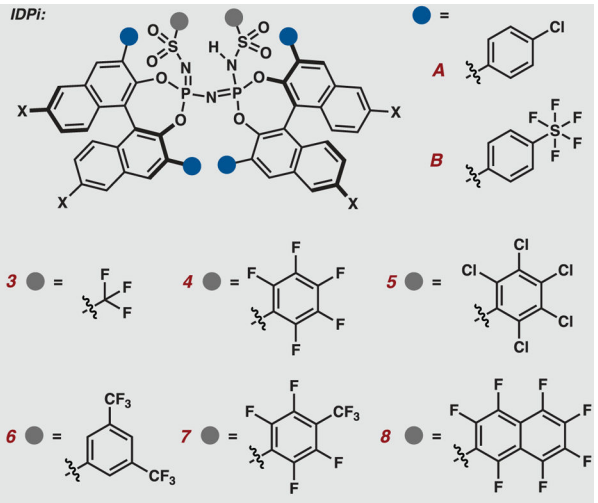

Yields determined by ^{1}H NMR with an internal standard.

*Isolated yield on 0.1 mmol scale. conv., conversion of starting material; TIPS, triisopropylsilane; TMS, trimethylsilane.